RSC Advances

PAPER

View Article Online
View Journal | View Issue

Cite this: *RSC Adv.*, 2017, **7**, 35221

Nanostructured WO_3 photoanodes for efficient water splitting *via* anodisation in citric acid†

Jifang Zhang,[a] Ivette Salles,[b] Sam Pering,[c] Petra J. Cameron,[c] Davide Mattia[a] and Salvador Eslava*[a]

In this work we report the production of nanostructured WO_3 photoanodes for solar water splitting produced *via* anodisation using for the first time citric acid (CA), a safer and more environmentally friendly alternative to fluoride-based electrolytes. Photoelectrochemical solar water splitting has shown potential as a renewable method for hydrogen production, a key ingredient to advance the decarbonisation of our economy. Many methods to produce WO_3 photoanodes are time-consuming and require high temperatures and/or toxic chemicals, such as fluoride-based electrolytes. Here we report on a systematic investigation of the anodisation of tungsten using CA to establish a relation between (i) anodisation parameters (current, time and electrolyte), (ii) the resulting nanostructured morphology and (iii) its performance as a photoanode for water splitting. Characterisation was carried out by X-ray diffraction, scanning electron microscopy, linear sweep voltammetry, and ultraviolet-visible spectroscopy. After optimisation, the obtained WO_3 photoanodes produced a photocurrent of 0.88 mA cm^{-2} at 1.0 V *vs.* Ag/AgCl in 0.5 M aqueous H_2SO_4 under AM1.5 solar irradiation. At low applied potentials (below 0.67 V *vs.* Ag/AgCl), closer to practical conditions, the photoanodes produced in CA outperformed a conventional counterpart made using a NH_4F electrolyte. The CA-anodised photoanodes also showed higher stability, retaining 90% of their activity after 1 h of chopped solar illumination. This work demonstrates the promise of anodisation in citric acid as an efficient and more sustainable method for the production of WO_3 photoanodes for solar water splitting.

Received 11th May 2017
Accepted 6th July 2017

DOI: 10.1039/c7ra05342h

rsc.li/rsc-advances

Introduction

Photoelectrochemical (PEC) water splitting is a promising approach to produce hydrogen, a sustainable clean fuel, and significant progress has been made since its first advent.[1] In a PEC cell, the choice of materials for electrodes is essential. Among different metal oxide semiconductors, tungsten trioxide (WO_3) has received much attention due to its band gap of 2.7 eV within the visible-light region, the relatively long diffusion length (150 nm) of its hole carriers, and its excellent stability in acidic conditions.[2] Many methods, including chemical vapour deposition, solvothermal, sol–gel and anodisation have been deployed to produce nanostructured WO_3.[3–10] Their optimised performance is associated with the production of larger active surface areas, better light harvesting capability, and more effective transport of charge carriers. However, many deposition methods such as chemical vapour deposition and flame deposition involve complex experimental setups or conditions which compromise the large scale production.[3,4] Sol–gel and solvothermal methods are relatively simpler to carry out, and WO_3 nanostructures can be formed too with careful selection of solvents and reaction conditions.[5–8] Nevertheless, long hours at high temperatures are often required. Anodisation, compared to other preparation techniques for photoelectrodes, is inexpensive and simple, making it suitable for large scale fabrication. It consists of growing a natural oxide layer of a metal foil by electrolytic passivation, followed by crystallisation at adequate temperatures (typically 400 to 600 °C). As the metal oxide layer grown on top is tightly bound to the metal support, the efficacy of charge collection is high. However, there is one major disadvantage in the anodisation of tungsten. Current reports exclusively use electrolytes that contain one or more fluorides (*e.g.* NaF, HF or NH_4F) as etching agents, which potentially bring serious safety issues due to the presence or formation of HF.[9,11–13] Few F-free alternative electrolytes have been reported to successfully anodise tungsten, such as oxalic acid and NH_4NO_3, which have shown highly porous nanostructures.[14,15] Therefore, it is meaningful to explore more F-free electrolytes and approaches for safer, faster and more scalable anodisation for the production of WO_3 photoanodes.

[a]*Department of Chemical Engineering, University of Bath, Bath, UK. E-mail: s.eslava@bath.ac.uk*

[b]*Departament d'Enginyeria Química, Biològica i Ambiental, Universitat Autònoma de Barcelona, Bellaterra 08193, Spain*

[c]*Department of Chemistry, University of Bath, BA2 7AY, UK*

† Electronic supplementary information (ESI) available: FESEM micrographs, XRD patterns and photocurrent density measurements. See DOI: 10.1039/c7ra05342h

An ideal anodising electrolyte for the formation of photoanodes needs to assist the oxidation of the top surface of the precursor metal foil under an electric field and promote a morphology and porosity that eventually enhance the photoresponse. Citric acid (CA, $C_6H_8O_7$) is known for its chelating properties and is widely used to soften water due to its ability to bind metals.[16] It is also used as a structure-directing agent in solution-based synthesis methods.[17,18]

Here, we demonstrate for the first time that CA offers a sustainable, fast and effective replacement of fluoride-containing electrolytes for the anodisation of tungsten foil and the preparation of nanostructured WO_3 photoanodes for solar water splitting. We report the results of different anodising conditions using CA and compare the performance of the resulting photoanodes with that using NH_4F as electrolyte. The comparison is made by analyses of their structural as well as photoelectrochemical properties, including photocurrent density under solar simulation measured by linear sweep voltammetry (LSV), applied bias photon-to-current efficiency (ABPE), and incident photon-to-current conversion efficiency (IPCE). The stability of the photoanodes is also tested.

Experimental

Materials

Tungsten foil (0.1 mm, 99.95%) was purchased from Alfa Aesar. Citric acid (CA, 99%) and *N*-methylformamide (NMF, 99%) were purchased from Sigma-Aldrich. Ammonium fluoride (NH_4F, 98+%) and sulfuric acid (H_2SO_4, 5 M) were supplied by Acros Organics and Fluka Analytical, respectively. Analytical acetone was obtained from VWR Chemicals and deionised water was used.

Anodisation

Tungsten foil was cut into 15 × 30 mm rectangles and sonicated for 15 minutes in acetone. After sonication, the foil pieces were rinsed with H_2O and dried under pressurised air. The anodisation was carried out by using the cleaned foil pieces as the anode of a two-electrode cell and a 3 mm-thick stainless steel piece as the cathode. Teflon and rubber templates were used to limit the anodisation to a circular area of 13 mm in diameter. The anode and cathode were held in parallel at a distance of 10 mm and immersed in electrolytes consisting of 0.1 M CA in either H_2O or a solution of 80 vol% NMF and 20 vol% H_2O. A jacketed beaker connected to a refrigerated circulating bath (DC-10, Thermo) kept the electrolyte at a constant temperature of 0 °C. Samples were anodised for 30 minutes at constant currents, controlled by a DC power supply (Agilent 6675A). One of the previously published procedures using fluoride electrolyte[10] was repeated for comparison: tungsten pieces were anodised for 6 h under 40 V at 40 °C in NMF solution including 20 vol% H_2O and 0.05 wt% NH_4F. After anodisation, all samples were rinsed with H_2O, dried in air, and calcined in air at 450 °C for 4 h.

Physical characterisations

Morphology of photoanodes after fabrication processes was characterised by Field Emission Scanning Electron Microscopy (FESEM), JEOL 6301F, with an acceleration voltage of 5 keV. Film thicknesses were measured at ten different sites to calculate the mean value and standard deviation (quoted with a ± sign). Area fraction is measured using ImageJ. X-ray diffraction was performed with a BRUKER AXS D8 advance diffractometer using a Vantec-1 detector and CuKα radiation.

Photoelectrochemical performance

Photoelectrochemical measurements were carried out in a three-electrode photoelectrochemical quartz cell using the prepared WO_3 electrode as the working electrode, a Pt wire counter electrode, a Ag/AgCl (in 3.5 M KCl) reference electrode, and 0.5 M H_2SO_4 electrolyte. Solar simulated light on an 8 mm-diameter area was provided by a 300 W Xe Lamp (LOT Quantum Design) equipped with an AM1.5G filter. The irradiation intensity was set to 1 sun (100 mW cm^{-2}). An external potential (provided by Ivium CompactStat) was linearly swept from 0 to 1.2 V *vs.* Ag/AgCl at a rate of 20 mV s^{-1}. Applied bias photon-to-current efficiency (ABPE) was obtained using the following equation:

$$\mathrm{ABPE} = \left[\frac{\left|j_{\mathrm{ph}}\ (\mathrm{mA\ cm^{-2}})\right| \times \left(E_{\mathrm{H_2O/O_2}} - |V_{\mathrm{b}}|\right)\ (\mathrm{V})}{P_{\mathrm{total}}\ (\mathrm{mW\ cm^{-2}})}\right]_{\mathrm{AM1.5G}}$$

where j_{ph} is the net photocurrent density measured at an applied bias V_{b} and P_{total} is the total solar incident irradiation.

Incident photon-to-current efficiency (IPCE) measurements were performed from 300 to 500 nm with the same light source and a triple grating Czerny-Turner monochromator. The intensity of monochromatic light was measured at the working electrode position with a SEL033/U photodetector (International Light Technologies). The values of IPCE were then calculated using the formula below:

$$\mathrm{IPCE}(\lambda) = \frac{\left|j\ (\mathrm{mA\ cm^{-2}})\right| \times 1239.8\ (\mathrm{V\ nm})}{P_{\mathrm{mono}}\ (\mathrm{mW\ cm^{-2}}) \times \lambda\ (\mathrm{nm})}$$

where j is the photocurrent density measured under single wavelength (λ) light illumination and P_{mono} is its incident irradiation power.

Photoelectrochemically active surface area (PECSA) values were calculated by measuring double layer capacitances with cyclic voltammetry. Potential was scanned at rates from 5 to 160 mV s^{-1} in a window of 0.2 V around open-circuit potential. The active surface area was then calculated using equation: PECSA = $C_{\mathrm{DL}}/C_{\mathrm{S}}$,[19] where C_{DL} is the slope for the fitted line plotted from measured currents against scanning rates, and C_{S} (specific capacitance) took the value of the unit area C_{DL} for a photoanode that has compact oxide layer produced from a controlled weak anodisation. The same electrochemical and light irradiation setup used for photocurrent density measurements was also used herein.

Results and discussion

Anodisation was carried out in two selected types of solvents: H_2O and a mixture of NMF and H_2O. NMF is added for its high dielectric constant which can favour higher charge density and

assist oxide growth,[20] and H_2O is added as an oxygen donor and to assist the dissolution of CA, which is not soluble in NMF and unstable in other anodising solvents such as ethylene glycol or glycerol. Although it is sometimes argued that H_2O concentration should be minimal for fast and deep anodisation and that H_2O content in air is sufficient to act as oxygen source, adding H_2O ensures the formation of a porous oxide.[12,21] We used a mixture of H_2O and NMF in a 20 and 80 vol% proportion, as this was found to be optimal by Tacca *et al.*[10] The same solvents were used with NH_4F for reference of the effectiveness of CA as etching agent.

The morphology of WO_3 films on the tungsten foil surface after anodisation was examined by FESEM. In the H_2O solution, the CA-assisted anodisation etched the tungsten foil into a canyon-like nanostructure with valleys and corrugated WO_3 walls and rods occupying approximately 70% of the area (Fig. 1a and b). This differs from the commonly seen WO_3 mesoporous mesh-like structures observed after anodisation in fluoride-containing media.[9,11–13] The height of the nanostructured valleys is estimated to be around 500 nm, below which there is a thin, compact layer of WO_3, which adds up to a total thickness of *ca.* 3.7 ± 1.5 μm (Fig. S1a, ESI†). The width of the walls and rods are between 100 and 200 nm. It is worth noting that their corrugated features should allow for stronger light scattering and absorption, as has been demonstrated in WO_3 photoanodes with helical nanostructure produced with oblique angle deposition.[22]

The etching of the tungsten foil top surface during the anodisation in CA/H_2O was investigated at different times by FESEM to understand the formation of the canyon-like nanostructure. First, a compact layer of tungsten oxide is formed under electrochemical oxidation, where cracks appear due to the difference in density of the oxide layer compared to tungsten, inducing strong local stresses (Fig. S2a†). Next, field-assisted dissolution starts to play an important role in the vicinity of the cracks, rendering the formation of holes of several hundred nanometres across (Fig. S2b†). The relatively compact oxide is then carved into nanowalls/nanorods (Fig. S2c†). The existence of nanorods is a result of horizontal dissolution as demonstrated by the "natural bridges" between two nanorods on the top right corner of Fig. 1a inset. Extended anodisation time can cause total dissolution of tungsten foil and hence a less effective working area. (Fig. S2d†). The morphological migration observed here is akin to the formation mechanism proposed by Chai and co-workers using oxalic acid anodisation, although they obtained a different porous structure consisting of spherical voids.[23]

The morphology can also be controlled by changing the anodisation current. Results for a series of specimens anodised at different current values (0.05, 0.08 and 0.10 A) for 30 min indicate further features in the formation of the WO_3 layer (Fig. 2). When anodised at 0.05 A, cracks (deep valleys) dominate the morphology of the layer, which appears to be rougher and with a less uniform porosity (Fig. 2a). At 0.08 A, more shallow valleys spread over the majority of the surface, with relatively limited flat domains (Fig. 2b). Anodisation at 0.10 A obtains the most uniform porosity and finer features (Fig. 2c). Above 0.10 A, large cavities up to 100 μm arise due to pitting corrosion (Fig. 2d). The higher porosity gained from nanorods/nanowalls compared to other structures is beneficial for its photoresponse.

The morphology of CA-anodised films was found to depend also on the choice of solvents. When anodised in CA/NMF/H_2O, a different morphology was obtained where nanowires of *ca.* 50 nm in diameter with different lengths and random orientation are predominant (Fig. 1c and d). This indicates that the high dielectric constant of NMF solvent compared to water has an effect on the final morphology.

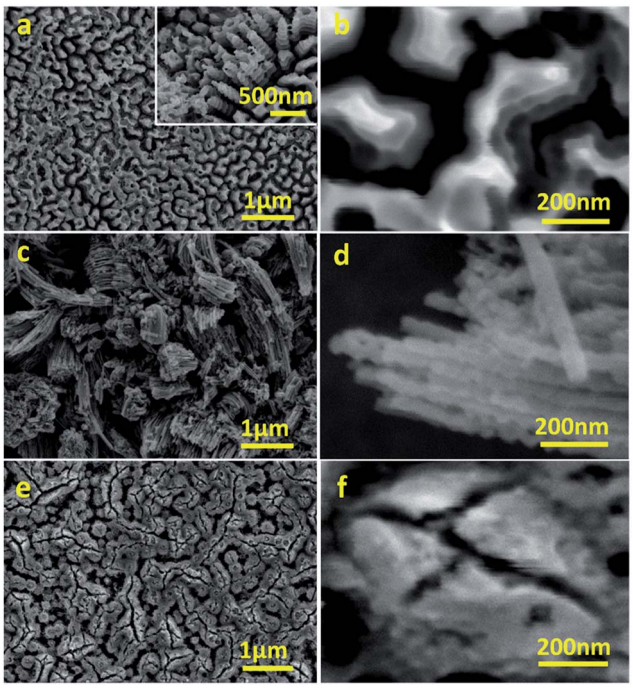

Fig. 1 Representative FESEM micrographs of WO_3 photoanodes anodised in CA/H_2O at 0.1 A for 30 min (a, b), in CA/NMF/H_2O at 0.015 A for 30 min (c, d), and in NH_4F/NMF/H_2O at 40 V for 6 h (e, f).

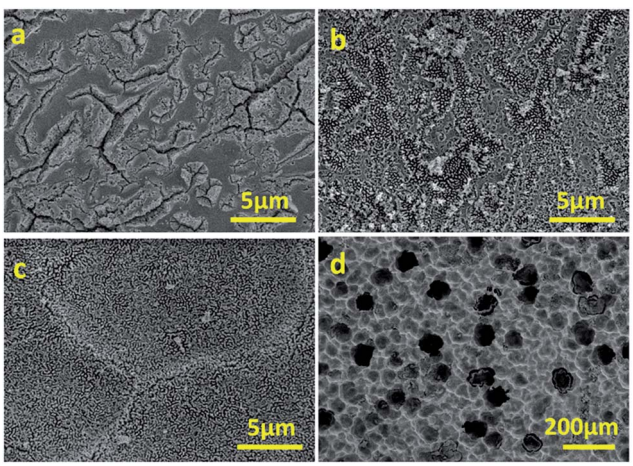

Fig. 2 FESEM micrographs of photoanodes after anodisation in CA/H_2O for 30 min at 0.05 A (a), 0.08 A (b), 0.10 A (c) and 0.15 A (d).

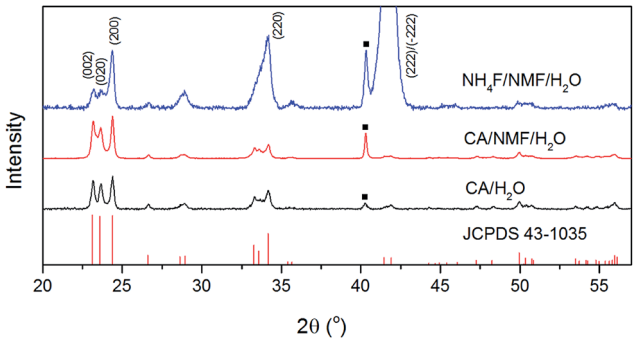

Fig. 3 XRD patterns of calcined WO_3 photoanodes anodised in CA/H_2O at 0.1 A for 30 min (black), in CA/NMF/H_2O at 0.015 A for 30 min (red), and in NH_4F/NMF/H_2O at 40 V for 6 h (blue) with reference to monoclinic WO_3 (JCPDS no. 43-1035). Squares indicate diffraction from metallic tungsten (110) under WO_3.

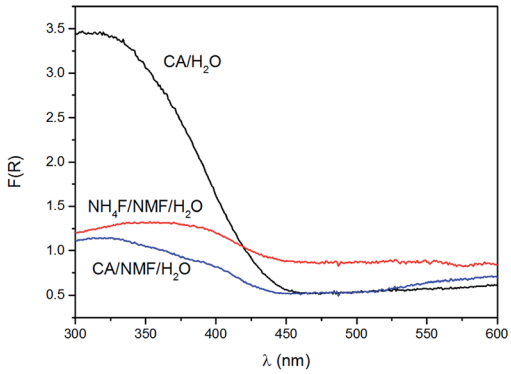

Fig. 4 Kubelka–Munk function, $F(R)$, of films anodised in CA/H_2O at 0.1 A for 30 min (black), in CA/NMF/H_2O at 0.015 A for 30 min (blue), and in NH_4F/NMF/H_2O at 40 V for 6 h (red) obtained from UV-visible diffuse reflectance spectroscopy.

For comparison to literature, we anodised the same tungsten foil in NH_4F/NMF/H_2O and obtained a worm-like porous morphology (Fig. 1e and f), as reported in the literature, different to the canyon-like nanostructure or the nanowire structures obtained with CA.[10] Cross sectional FESEM micrographs show that the thicknesses of the films under study are *ca.* 5.8 ± 1.7 μm for CA/NMF/H_2O anodised film and *ca.* 7.4 ± 2.7 μm for NH_4F/NMF/H_2O anodised film (Fig. S1b and c†). Therefore, CA has a similar etching capability with NH_4F, despite the citrate ligand being bulkier.

Fig. 3 shows the XRD patterns of anodised films after calcination. The phases of the oxide layer in all cases are monoclinic (JCPDS no. 43-1035), which is the typical phase encountered upon various anodisation methods[10,12–14,24] and has proved to be superior to other phases including orthorhombic and hexagonal in photocatalysis.[25] Despite the fact that calcination temperature and dwell time are the same, the oxide formed using NH_4F as electrolyte has preferential orientation along (−222)/(222), which was also observed elsewhere and found to be the most stable orientation during aging tests.[10,26] Notably, the calcination step after anodisation is essential because for uncalcined photoanodes, the oxide formed has poor crystallinity and is not photoresponsive (see Fig. S3†).

Kubelka–Munk conversion of UV-visible diffuse reflectance spectroscopy of anodised films after calcination is shown in Fig. 4. All anodised films show the WO_3 bandgap absorbing at wavelengths below 450 nm. For wavelengths above 450 nm, the NH_4F/NMF/H_2O anodised films absorb more light, which could be due to F doping originated from the electrolyte, as observed in F-doped TiO_2 powders.[27] Lower, but still evident is the absorption at those high wavelengths in CA/H_2O and CA/NMF/H_2O films, which could be due to minor carbon doping from CA or NMF. Although the Kubelka–Munk conversion compensates for specular reflectance, this cannot be completely ruled out in these measurements.

Anodised films were tested for photoelectrochemical water splitting. The photocurrent densities under solar illumination measured on films are found to be optimal when anodised at 0.1 A for 30 min in CA/H_2O and 0.015 A for 30 min in CA/NMF/H_2O (Fig. S4†). Fig. 5a shows representative LSV curves of these optimised WO_3 films, with or without solar illumination in a three-electrode system. In spite of differences in WO_3 thickness between the CA/H_2O- and the CA/NMF/H_2O-anodised photoanodes (3.7 ± 1.5 *vs.* 5.8 ± 1.7 μm, resp.), they show similar performance: the net photocurrent densities measured at 1.0 V *vs.* Ag/AgCl in 0.5 M H_2SO_4 are 0.88 mA cm^{-2} and 0.77 mA cm^{-2}, respectively. This could be assigned to a stronger light scattering effect in the corrugated canyon-like nanostructure (formed in CA/H_2O) compared to the thin nanowires (formed in CA/NMF/H_2O). Another cause is that the ordered structure favours a more facile charge collection between the oxide and the metal basis than the randomly oriented nanowires. These values are comparable with published data for fluoride-based anodisations,[12,13,24] while using a more benign electrolyte. The film prepared with NH_4F/NMF/H_2O, used here

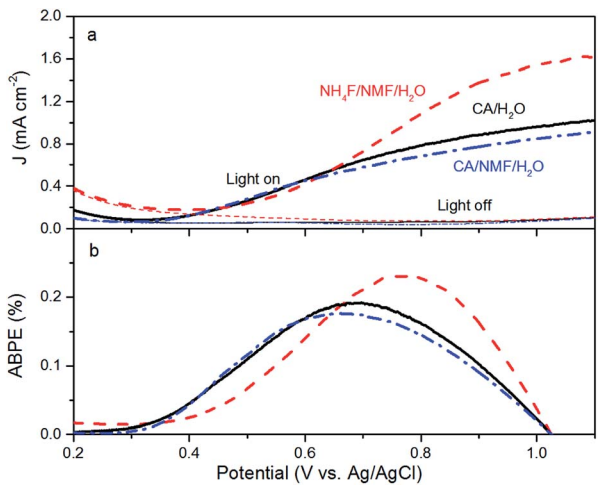

Fig. 5 (a) Current densities of WO_3 photoanodes in the presence and absence of AM1.5G illumination (100 mW cm^{-2}). (b) Calculated ABPE of WO_3 electrodes. Electrodes were prepared by anodising tungsten foils in CA/H_2O at 0.1 A for 30 min (black solid line), in CA/NMF/H_2O at 0.015 A for 30 min (blue dash-dot line), and in NH_4F/NMF/H_2O at 40 V for 6 h (red dashed line).

as a competitive benchmark, showed a higher photocurrent at 1 V *vs.* Ag/AgCl. Accordingly, ABPE values show higher efficiencies below 0.67 V *vs.* Ag/AgCl for CA-anodised samples (Fig. 5b). These differences can be ascribed to their different morphology and crystal orientation, observed by FESEM and XRD, which could affect their light absorption, charge transfer efficiency, and amount of surface states. One should note that a higher response at lower onset potential can be advantageous for tandem PEC cells working with little or no applied potentials.

The trends from LSV measurements were further confirmed by IPCE measured at 0.55 V and 1 V *vs.* Ag/AgCl (Fig. 6a). Photoanodes prepared using CA have similar performance at both conditions and at all wavelengths. When NH_4F was used, the response was not as high as using CA at 0.55 V *vs.* Ag/AgCl, which is consistent with the photocurrent and ABPE results in Fig. 4. Tauc plot based on IPCE spectra at 1 V *vs.* Ag/AgCl shows estimated band gaps of about 2.7 eV for all three photoanodes (Fig. 6b). It is notable that at 1 V *vs.* Ag/AgCl there is an IPCE maximum between 350 and 420 nm, centred at 375 nm, for WO_3 prepared in NH_4F/NMF/H_2O. This IPCE maximum is not present at 0.55 V *vs.* Ag/AgCl for the same film. This agrees with and confirms the higher photocurrent density observed in LSV measurements at higher applied potentials.

The stability of WO_3 photoanodes was tested at 1 V *vs.* Ag/AgCl in 0.5 M H_2SO_4 solution for 60 min with 6 min cycles of light chopping (Fig. 7). The photoanode anodised in CA/H_2O shows a decay of 0.14 mA cm^{-2} in photocurrent density within the first two cycles, which can be attributed to photoelectrochemical instability caused by corrosion from accumulating holes at electrode–electrolyte interface.[27] After two cycles, the decay slows down and, overall, 69% of its initial stability is retained. For the CA/NMF/H_2O anodised sample, 90% of its initial photoresponse is maintained after the test. We attribute this superior result to its morphology consisting of thin nanowires having a higher photoelectrochemically active surface area (3.8 cm^2 *vs.* 1.7 cm^2), which is in favour of faster charge transfer. This leads to less accumulation of holes at the semiconductor–liquid junction and thereby higher photoelectrochemical stability.[28] On the other hand, for the sample anodised in NH_4F/NMF/H_2O, poorer stability is observed. The photocurrent density suffers from gradual decline throughout the amount of time being tested, meaning a low photoelectrochemical stability. In addition, the photocurrent densities cannot reach its previous level after each dark period, which represents poor chemical stability. The photocurrent density is almost halved (53%) after one hour. Therefore, the stability test shows a clear advantage of CA-anodised photoanode over the fluoride-anodised photoanode.

The performance of several porous anodic WO_3 films is listed in Table 1 along with their synthesis and characterisation conditions. The nanowalls/nanorods structures formed here by CA anodisation in aqueous solution bear much resemblance to Ng's work where corrugated nanorods of 450 nm in height were

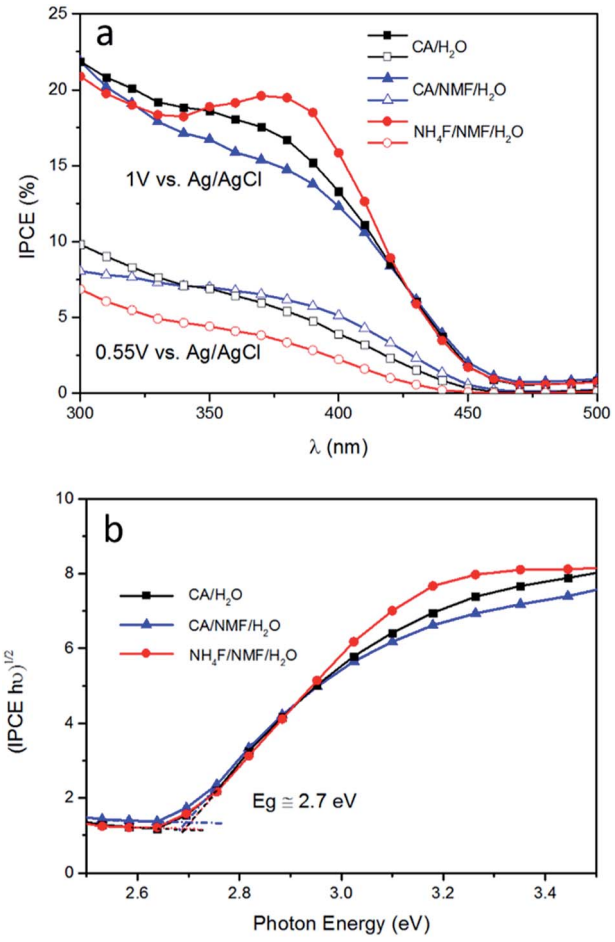

Fig. 6 (a) Incident photon-to-current conversion efficiency (IPCE) results for photoanodes subjected to anodisations in CA/H_2O at 0.1 A for 30 min (black squares), in CA/NMF/H_2O at 0.015 A for 30 min (blue triangles), and in NH_4F/NMF/H_2O at 40 V for 6 h (red circles). Filled shapes indicate measurements at an applied bias of 1 V and hollow shapes at 0.55 V *vs.* Ag/AgCl. Both measurements were carried out in 0.5 M H_2SO_4. (b) Band gaps for WO_3 on all photoanodes are estimated to be ~2.7 eV based on IPCE spectra at 1 V *vs.* Ag/AgCl.

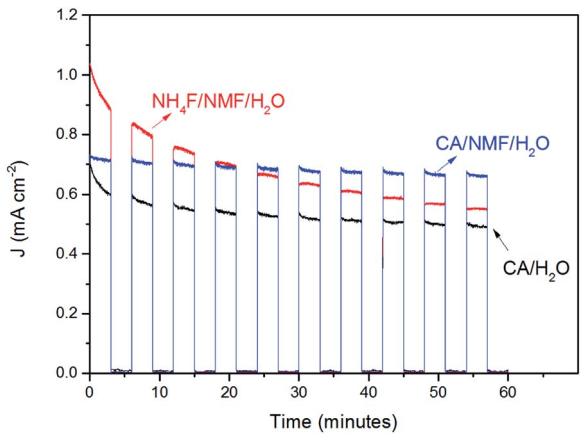

Fig. 7 Stability test of WO_3 electrodes prepared using CA/H_2O at 0.1 A for 30 min (black), in CA/NMF/H_2O at 0.015 A for 30 min (blue), and in NH_4F/NMF/H_2O at 40 V for 6 h (red) at 1 V *vs.* Ag/AgCl in 0.5 M H_2SO_4 under AM1.5G illumination (100 mW cm^{-2}). Light was chopped with 3 min intervals.

Table 1 Properties of photoanodes formed by various anodisation methods[a]

Anodising media	Anodising voltage and time	Morphology	Phase	Electrolyte	J (mA cm^{-2}) at 1.23V_{RHE}	Onset (V) *vs.* RHE	Light source and intensity
80 v% NMF/20 v% H_2O/0.05 wt% NH_4F[10]	40 V, 6 h	Crispy surface crust	Monoclinic	1 M H_2SO_4	3.6	0.5	AM1.5, 300 mW cm^{-2}
1.5 M HNO_3/40 mg NH_4F[24]	30 V, 4 h	Triple-layered	Monoclinic	0.5 M Na_2SO_4	0.9	0.4	Xe lamp, 100 mW cm^{-2}
0.1 M NaF[12]	60 V, 24 h	Mesh-like	Monoclinic	0.1 M HCl	0.75	0.45	AM1.5, 100 mW cm^{-2}
1 M Na_2SO_4/ 0.5 wt% NaF[29]	50 V, 30 min	Mesh-like	n.d.	0.5 M H_2SO_4	1.0	0.6	Xe lamp λ > 400 nm, 100 mW cm^{-2}
0.1 M Na_2SO_4/ 0.5 wt% NaF[13]	50 V, 30 min	Mesh-like	Monoclinic	0.1 M KH_2PO_4 + KOH (pH 7)	0.9	0.7	AM1.5, 100 mW cm^{-2}
0.2 M NH_4NO_3/ ethylene glycol[14]	10 V, 35 min	Nanochannel	Monoclinic	0.5 M Na_2SO_4 + 0.1 M HCOONa	2.5	0.52	AM1.5, 100 mW cm^{-2}
0.1 M CA (this work)	0.1 A 30 min	Nanowalls/ nano-rods	Monoclinic	0.5 M H_2SO_4	0.88	0.5	AM1.5, 100 mW cm^{-2}

[a] Photocurrent densities and onset potentials listed were approximatively read on figures from references.

obtained using Na_2SO_4 and NaF as an electrolyte.[30] Moreover, the reported formation process is similar to that observed herein, which proves the success of CA as an effective electrolyte to replace fluorides. Fluoride-free anodisations have been explored in other works, with the formation of WO_3 layers with different morphologies and dimensions. For example, a slow growth of a "nanosponge" was achieved in a 10 wt% K_2HPO_4/ glycerol electrolyte.[15] The thickness was up to 8.7 μm for a long 26 h anodisation. A 7.5 μm film of WO_3 nanotubes was reported for 0.2 M NH_4NO_3/ethylene glycol by Wei *et al.*[14] The plateau photocurrent density under solar irradiation was 2.5 mA cm^{-2} in the presence of HCOONa as a hole scavenger. More ordered and higher-aspect-ratio nanotubes were also recently formed anodising in molten H_3PO_4, although no photoresponse was reported.[31] To the best of our knowledge, the present work is the first to report the formation of WO_3 nanostructures using CA.

Conclusion

In this work, citric acid (CA) was studied for the anodisation of tungsten foil as an alternative to fluoride-based electrolytes such as NH_4F. A systematic investigation of anodisation process parameters (time, currents and solvents) was performed to establish a relation between the obtained morphology and its performance in solar water splitting. We demonstrated, for the first time, that a CA/H_2O electrolyte can produce porous canyon-like nanostructure consisting of WO_3 nanowalls and nanorods. Using a mixture of CA, H_2O and NMF, a different porous nanostructure was obtained consisting of randomly oriented ~50 nm wide WO_3 nanowires. These morphologies differ from the classic mesh-like porous nanostructures obtained with NH_4F as an anodising electrolyte. The performance of these anodised films was tested for photoelectrochemical water splitting using a three-electrode system and simulated sunlight. The CA-anodised films obtained photocurrent densities around 0.8 mA at 1 V *vs.* Ag/AgCl in 0.5 M H_2SO_4. These CA-anodised films outperformed NH_4F-anodised films at low applied potentials (below 0.67 V *vs.* Ag/AgCl) and showed much better photoelectrochemical stability. As such, CA represents a safer and more environmentally friendly alternative to fluoride-based electrolytes for the production of nanostructured WO_3 photoanodes with comparable or superior performance. This work also opens an avenue for sustainable anodisation procedures for the production of other nanostructured metal oxides as photoelectrodes using CA.

Acknowledgements

SE would like to acknowledge the financial support from EPSRC (EP/P008097/1).

References

1 A. Fujishima and K. Honda, *Nature*, 1972, **238**, 37.
2 J. Lin, P. Hu, Y. Zhang, M. Fan, Z. He, C. K. Ngaw, J. S. C. Loo, D. Liao and T. T. Y. Tan, *RSC Adv.*, 2013, **3**, 9330.
3 J. Ding and K. Kim, *J. Nanosci. Nanotechnol.*, 2016, **16**, 1578.
4 V. Chakrapani, J. Thangala and M. K. Sunkara, *Int. J. Hydrogen Energy*, 2009, **34**, 9050.
5 C. Santato, M. Odziemkowski, M. Ulmann and J. Augustynski, *J. Am. Chem. Soc.*, 2001, **123**, 10639.
6 J. Su, X. Feng, J. D. Sloppy, L. Guo and C. A. Grimes, *Nano Lett.*, 2011, **11**, 203.
7 D. Qin, C. Tao, S. A. Friesen, T. Wang, O. K. Varghese, N. Bao, Z. Yang, T. E. Mallouk and C. A. Grimes, *Chem. Commun.*, 2012, **48**, 729.
8 Y. Hou, F. Zuo, A. P. Dagg, J. Liu and P. Feng, *Adv. Mater.*, 2014, **26**, 5043.
9 A. Watcharenwong, W. Chanmanee, N. R. de Tacconi, C. R. Chenthamarakshan, P. Kajitvichyanukul and K. Rajeshwar, *J. Electroanal. Chem.*, 2008, **612**, 112.
10 A. Tacca, L. Meda, G. Marra, A. Savoini, S. Caramori, V. Cristino, C. A. Bignozzi, V. Gonzalez Pedro, P. P. Boix, S. Gimenez and J. Bisquert, *ChemPhysChem*, 2012, **13**, 3025.
11 N. R. De Tacconi, C. R. Chenthamarakshan, G. Yogeeswaran, A. Watcharenwong, R. S. De Zoysa, N. A. Basit and K. Rajeshwar, *J. Phys. Chem. B*, 2006, **110**, 25347.

12 K. R. Reyes-Gil, C. Wiggenhorn, B. S. Brunschwig and N. S. Lewis, *J. Phys. Chem. C*, 2013, **117**, 14947.
13 Q. Liu, Q. Chen, J. Bai, J. Li, J. Li and B. Zhou, *J. Solid State Electrochem.*, 2014, **18**, 157.
14 W. Wei, S. Shaw, K. Lee and P. Schmuki, *Chem.–Eur. J.*, 2012, **18**, 14622.
15 W. Lee, D. Kim, K. Lee, P. Roy and P. Schmuki, *Electrochim. Acta*, 2010, **56**, 828.
16 K. Kirimura, Y. Honda and T. Hattori, *Compr. Biotechnol.*, 2011, **3**, 135.
17 Q. Han, X. Wu, Y. Liao, D. Li, R. Yue, H. Liu and Y. Chen, *Mater. Lett.*, 2013, **95**, 9.
18 A. E. Danks, S. R. Hall and Z. Schnepp, *Mater. Horiz.*, 2016, **3**, 91.
19 S. Trasatti and O. A. Petrii, *Pure Appl. Chem.*, 1991, **63**, 711.
20 V. Cristino, S. Caramori, R. Argazzi, L. Meda, G. L. Marra and C. A. Bignozzi, *Langmuir*, 2011, **27**, 7276.
21 M. Paulose, K. Shankar, S. Yoriya, H. E. Prakasam, O. K. Varghese, G. K. Mor, T. A. Latempa, A. Fitzgerald and C. A. Grimes, *J. Phys. Chem. B*, 2006, **110**, 16179.
22 X. Shi, I. Y. Choi, K. Zhang, J. Kwon, D. Y. Kim, J. K. Lee, S. H. Oh, J. K. Kim and J. H. Park, *Nat. Commun.*, 2014, **5**, 4775.
23 Y. Chai, C. W. Tam, K. P. Beh, F. K. Yam and Z. Hassan, *J. Porous Mater.*, 2013, **20**, 997.
24 H. Qi, J. Wolfe, D. Wang, H. J. Fan, D. Fichou and Z. Chen, *Nanoscale*, 2014, **6**, 13457.
25 S. S. Kalanur, Y. J. Hwang, S. Y. Chae and O. S. Joo, *J. Mater. Chem. A*, 2013, **1**, 3479.
26 P. Dias, T. Lopes, L. Meda, L. Andrade and A. Mendes, *Phys. Chem. Chem. Phys.*, 2016, **18**, 5232.
27 T. W. Kim and K. S. Choi, *J. Phys. Chem. Lett.*, 2016, **7**, 447.
28 D. Bae, B. Seger, P. C. K. Vesborg, O. Hansen and I. Chorkendorff, *Chem. Soc. Rev.*, 2017, **46**, 1933.
29 W. Li, J. Li, X. Wang, S. Luo, J. Xiao and Q. Chen, *Electrochim. Acta*, 2010, **56**, 620.
30 C. Y. Ng, K. Abdul Razak and Z. Lockman, *J. Porous Mater.*, 2015, **22**, 537.
31 M. Altomare, O. Pfoch, A. Tighineanu, R. Kirchgeorg, K. Lee, E. Selli and P. Schmuki, *J. Am. Chem. Soc.*, 2015, **137**, 5646.